Production and Stabilization of a Spin Mixture of Ultracold Dipolar Bose Gases

Maxime Lecomte, Alexandre Journeaux, Julie Veschambre, Jean Dalibard, and Raphael Lopes*
Laboratoire Kastler Brossel, Collège de France, CNRS, ENS-Université PSL, Sorbonne Université, 11 Place Marcelin Berthelot, 75005 Paris, France

(Received 14 July 2024; accepted 3 December 2024; published 3 January 2025)

Mixtures of ultracold gases with long-range interactions are expected to open new avenues in the study of quantum matter. Natural candidates for this research are spin mixtures of atomic species with large magnetic moments. However, the lifetime of such assemblies can be strongly affected by the dipolar relaxation that occurs in spin-flip collisions. Here we present experimental results for a mixture composed of the two lowest Zeeman states of ^{162}Dy atoms, that act as dark states with respect to a light-induced quadratic Zeeman effect. We show that, due to an interference phenomenon, the rate for such inelastic processes is dramatically reduced with respect to the Wigner threshold law. Additionally, we determine the scattering lengths characterizing the *s*-wave interaction between these states, providing all necessary data to predict the miscibility range of the mixture, depending on its dimensionality.

DOI: 10.1103/PhysRevLett.134.013402

In the last decade, long-range interactions have become a central focus for quantum simulation [1–4]. From arrays of Rydberg atoms trapped in optical tweezers to the first observation of a dipolar molecular Bose-Einstein condensate (BEC) [5], a plethora of exciting new platforms are emerging. In this context, the manipulation of magnetic dipolar species such as erbium (Er) and dysprosium (Dy) has been particularly stimulating. This includes the observation of the roton instability [6], the control of infinite-range interactions in the synthetic dimension of dysprosium atoms [7], and the observation of supersolidity [8–15].

The possibility to create mixtures of dipolar gases opens a new route for studying the interplay between magnetic interactions, quantum fluctuations, and thermal effects. In these systems, a new interaction length scale arises due to interspecies interactions, similar to what is observed in alkali species that has led, for instance, to the observation of quantum liquid droplets [16,17]. Such mixtures are poised to exhibit a rich, as-yet-unexplored phase diagram [18], with the emergence of self-bound droplets [19] and spin-textured supersolids with multiple density-dependent spatial configurations [18–22]. Notably, binary dipolar Bose gases present a supersolid phase whose robustness is independent of quantum fluctuation effects, thus extending the parameter range, in terms of atom number, over which the supersolid clusters are stabilized [23–25].

The simultaneous manipulation of ultracold samples of erbium and dysprosium [26] holds promise for probing this rich physics, albeit at the cost of increased experimental complexity. A simpler alternative is the manipulation of dipolar spin mixtures [27–32]. However, the study of these mixtures has been hampered by two main factors. First, the large magnetic moment usually results in rapid dipolar relaxation processes for all Zeeman sublevels except the lowest energy one, rendering these systems intrinsically unstable [33–35]. Second, the apparently chaotic nature of the pairwise interactions in erbium and dysprosium, primarily due to their large anisotropic van der Waals coefficients [36–38], complicates the prediction of interaction sweet spots that would allow the exploration of different miscibility regimes in these mixtures. To date, only the interaction properties of the lowest-energy sublevel, for both erbium and dysprosium, have been characterized [39–45]. Efforts have been made to mitigate these factors, either through the preparation in a low magnetic field environment [46] or strong confinement in deep optical lattices [47].

In this Letter, we introduce a novel binary dipolar quantum gas composed of particles in the Zeeman sublevels $|J=8, m_J=-8\rangle$ and $|J=8, m_J=-7\rangle$ of ^{162}Dy (simply labeled hereafter as $|-8\rangle$ and $|-7\rangle$). We identify a magnetic field "sweet spot" where dipolar relaxation is suppressed by 2 orders of magnitude compared to the Wigner threshold law [48]. Combining our experimental results with a theoretical model of atomic interactions in this regime, and through the analysis of the BEC size scaling with atom number after time-of-flight (TOF) expansion, we determine the intraspecies scattering length $a_{77} = 110(10)a_0$ and the interspecies scattering length $a_{78} = 40(20)a_0$, where a_0 denotes the Bohr radius. These values, in combination with the already known $a_{88} = 140a_0$ [40,41] allow one to predict the stability diagram for the 7-8 mixture. Additionally, near this optimal magnetic field, we observe spin-dependent Feshbach resonances. These resonances provide precise control over the scattering

*Contact author: raphael.lopes@lkb.ens.fr

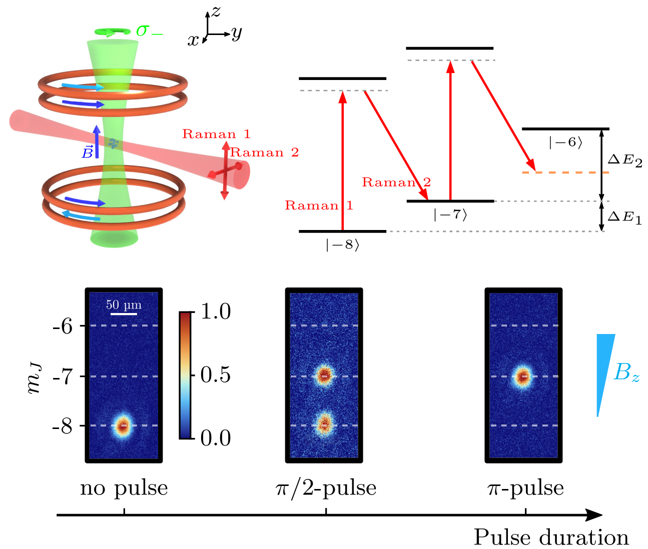

FIG. 1. Schematic representation of the experimental protocol. Top panels: two horizontal laser beams (Raman 1 and Raman 2) induce a Raman transition between nearest Zeeman sublevels. The vertical laser beam induces a spin-dependent light shift, allowing us to selectively couple the two lowest-energy Zeeman sublevels. Orange line represents the energy of $|-6\rangle$ in the absence of the light-induced quadratic Zeeman effect. Bottom panel: absorption images of Bose-Einstein condensates in different internal states, captured after time-of-flight (TOF) expansion in the presence of a magnetic field gradient. The rightmost absorption image corresponds to a BEC preparation in $|-7\rangle$ with purity $> 95\%$. Dashed lines serve as guides to the eye for the spatial position of atoms in states $|-8\rangle$, $|-7\rangle$, and $|-6\rangle$.

lengths [49], enabling the exploration of miscible-immiscible phases in binary dipolar condensates [25,50–52].

We first use an ultracold, but noncondensed, sample of ^{162}Dy. The temperature $T = 250$ nK is chosen to be high enough to avoid possible demixing effects. The gas is confined in an infrared, far-detuned, crossed dipole trap with angular frequencies $\{\omega_x, \omega_y, \omega_z\} = 2\pi \times \{38, 212, 172\}$ Hz. The samples are initially prepared in the lowest Zeeman sublevel $|-8\rangle$, in the presence of a magnetic field bias $\mathbf{B} = B\hat{z}$, and contain $\sim 10^5$ atoms (see Ref. [45] for details). Taking advantage of the nonzero tensorial part of the polarizability, we create a spin-dependent light shift via a laser beam (see Fig. 1), with radius at $1/e^2$ of 100 μm, propagating along the $\hat{z}$ direction, with σ^--polarization, blue detuned by $\Delta = 2\pi \times 2.5$ GHz from the $J' = J - 1$ optical transition at $\lambda = 530.305$ nm [53,54] (see also [55]). As a result, in the ground-state manifold, the energy of the different Zeeman sublevels is given up to a constant by

$$E(m_J) = \alpha m_J + \gamma(m_J + 7)(m_J + 8), \qquad (1)$$

where $\alpha = g_J \mu_B B$ is the Zeeman energy shift, g_J the Landé factor, and μ_B the Bohr magneton. We typically work with an optical power of 200 mW such that $\gamma/h \approx 30$ kHz. The chosen polarization ensures that the two lowest-energy Zeeman states $|-7\rangle$ and $|-8\rangle$ are uncoupled to the excited manifold, defining them as "dark states."

This nonlinear energy shift enables precise manipulation of the atomic sample between the $|-8\rangle$ and $|-7\rangle$ states. For this purpose, we use a two-photon Raman process facilitated by two copropagating laser beams with linear and orthogonal polarizations, detuned from the 626.1 nm atomic transition [56,57], with Rabi frequency $\Omega_R \approx 2\pi \times 23$ kHz. By performing a Rabi oscillation with adjustable duration, we can prepare either quasipure samples in $|-7\rangle$ or spin mixtures with adjustable amplitudes [28,31]. In Fig. 1, we present examples of absorption images of Bose-Einstein condensates (BECs) in different internal states, captured after time-of-flight in the presence of a magnetic field gradient.

Dipolar relaxation is the primary limitation in manipulating spin mixtures of strongly dipolar atomic gases. It is particularly pronounced in dysprosium due to its large magnetic moment [4]. At nonzero magnetic fields, only the state $|-8\rangle$, which is the lowest-energy Zeeman sublevel, is protected against dipolar relaxation; particles occupying any other internal state will eventually relax towards $|-8\rangle$. Let us consider the simplest relaxation process, where two particles collide, one in the internal state $|-8\rangle$ and the other in $|-7\rangle$. After collision, the particle initially in $|-7\rangle$ can spin-flip towards $|-8\rangle$, a process which we schematically represent by [see Fig. 2(a)]

$$|-7\rangle + |-8\rangle \to |-8\rangle + |-8\rangle. \qquad (2)$$

Because of momentum conservation, the two particles equally share the released Zeeman energy in the center-of-mass (c.m.) frame. For the magnetic fields used in this work, the released energy is much larger than the trap depth, resulting in the loss of both particles; for instance, at $B = 1$ G, $\Delta E \approx k_B \times 80$ μK, where k_B is the Boltzmann constant.

Experimentally, we probe this relaxation process by transferring a small fraction ($< 5\%$) of the ultracold sample into the internal state $|-7\rangle$ and holding the sample for a specified time. Subsequently, we measure the populations of both internal states $|-7\rangle$ and $|-8\rangle$, extracting the two-body loss rate L_2^{mix} from the time evolution of the minority component [see Fig. 2(a)]. We ensure that over the probed time, both the population and temperature of the atomic sample in $|-8\rangle$ remain constant within 20%. As shown in Fig. 2(b), we observe a non-monotonic evolution of L_2^{mix} with B over the range of 0.4 to 6 G. Remarkably, at $B \approx 2.5$ G, the measured loss rate is 2 orders of magnitude lower than the Wigner law prediction, which scales with magnetic field as $\sqrt{B}$ [33,35,48] [brown straight line in Fig. 2(b)].

To explain this spectacular reduction, we first recall the theoretical description, based on the Fermi golden rule

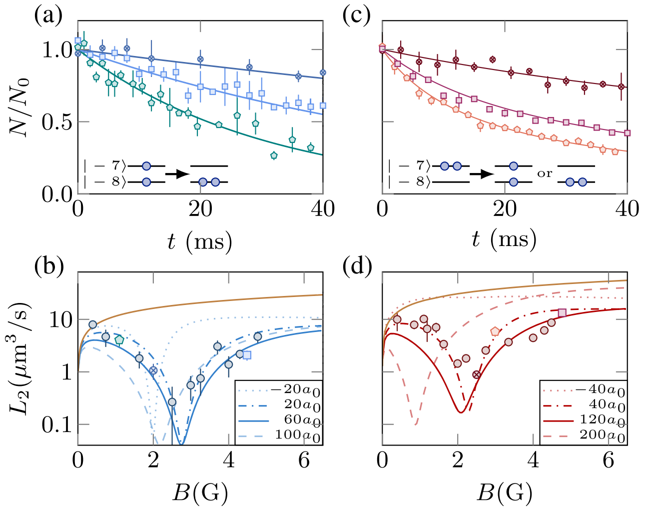

FIG. 2. Dipolar relaxation. Time evolution of the atom number in state $|-7\rangle$ for (a) minority component in $|-7\rangle$ ($<5\%$) immersed in the majority component $|-8\rangle$ (blue pentagon $B = 1.1$ G, blue crossed circle $B = 2.0$ G, and blue square $B = 4.5$ G) and for (c) pure sample in $|-7\rangle$ (red crossed circle $B = 2.5$ G, red pentagon $B = 3$ G and red square $B = 4.77$ G). (b) Two-body loss rate as a function of B for the case of a minority component in $|-7\rangle$. The lines correspond to theoretical predictions (see main text) for scattering length: $a_{78} = -20a_0$ (blue dotted line), $a_{78} = 20a_0$ (blue dash dot line), $a_{78} = 60a_0$ (blue line) and $a_{78} = 100a_0$ (dashed blue line). (d) Two-body loss rate as a function of B for the case of a pure sample in $|-7\rangle$. The lines correspond to theoretical predictions for scattering length: $a_{77} = -40a_0$ (red dotted line), $a_{77} = 40a_0$ (red dash dot line), $a_{77} = 120a_0$ (red line), and $a_{77} = 200a_0$ (red dashed line). The brown lines correspond to the Wigner law $\propto \sqrt{B}$.

(FGR) approach, of a dipolar relaxation process occurring between two atoms a and b. This process is induced by the dipolar interaction potential $V_{\rm dd}$, which is proportional to the scalar product of two rank-two tensor operators, $\mathcal{J}^{(2)}$ and $\mathcal{U}^{(2)}$, acting on the spin and orbital degrees of freedom of the two-particle system, respectively [58,59]:

$$V_{\rm dd} = -\frac{\alpha}{r^3}\sum_{m=-2}^{2}(-1)^m \mathcal{J}^{(2)}_{-m}\mathcal{U}^{(2)}_{m}. \tag{3}$$

The rank-two tensor operator $\mathcal{J}^{(2)} = (\boldsymbol{J}_a \otimes \boldsymbol{J}_b)^{(2)}$ is formed from the two rank-one spin operators $\boldsymbol{J}_a$ and $\boldsymbol{J}_b$. The rank-two orbital operator is defined by $\mathcal{U}^{(2)} = (\boldsymbol{u}\otimes\boldsymbol{u})^{(2)}$, with $\boldsymbol{u} = \boldsymbol{r}/r$ where $\boldsymbol{r} = \boldsymbol{r}_a - \boldsymbol{r}_b$ is the relative position variable. We set $\alpha = (3/8)^2\hbar^2 a_{\rm dd}/M$, where M is the atomic mass and $a_{\rm dd} = 129.2a_0$ is the so-called dipolar length [4], characterizing the strength of the dipolar interaction.

A single spin-flip process, which is the only one energetically allowed for the collision of Eq. (2), corresponds to the term $m = 1$ in the sum of Eq. (3). This term couples the initial s-wave scattering state $\psi_i(\boldsymbol{r})$ to a final d-wave state $\psi_f(\boldsymbol{r})$. The corresponding rate calculated using FGR reads [60]

$$L_2^{\rm mix} = \beta k_f\left[\int {\rm d}r\frac{1}{r}\chi_i(r)\chi_f(r)\right]^2, \tag{4}$$

where $\beta = 54\pi\hbar a_{\rm dd}^2/(5M)$, $\chi_{i/f}$ stand for the (real) radial parts of $\psi_{i/f}$ and $k_f = \sqrt{M\Delta E}/\hbar \propto \sqrt{B}$, where ΔE is the energy released in the spin flip process. In Eq. (4) the wave functions $\chi_{i/f}$ are normalized such that in the absence of interactions between a and b in input and output channels and in the limit of a zero initial energy, we have $\chi_i = 1$ and $\chi_f(r) = j_2(k_f r)$, where j_2 is the second spherical Bessel function of the first kind. We note that in this case, the integral entering in Eq. (4) does not depend on k_f, which leads to the Wigner threshold law $L_2^{\rm mix} \propto \sqrt{B}$.

Interactions in the input and output channels thus play a key role to understand the spectacular reduction of the rate $L_2^{\rm mix}$ observed in the experiment. Because of van der Waals and dipolar interactions, the wave functions $\chi_{i/f}(r)$ have several nodes in the region where $V_{\rm dd}$ is significant. A variation of the magnetic field B results in a shift of the nodes of χ_f with respect to those of χ_i and the integral entering Eq. (4) may thus vanish for a specific value of B (see also [55]). Physically, this integral can be viewed as the sum of the amplitudes of the paths $\chi_i \to \chi_f$, each path being labeled by the position r at which the spin flip process takes place. The situation for which the integral vanishes corresponds to a globally destructive interference between all these paths.

The full determination of the initial and final wave functions $\psi_{i/f}$ is a complex problem since the dipole interaction mixes all partial wave channels, leading to an infinite set of coupled-channel Schrödinger equations [36,61,62]. Here we adopt a semi-quantitative modeling with only one channel for the initial ($\ell = 0$) and for the final ($\ell = 2$) states. For each channel, we write the interaction potential $V(r) = V_{\rm cent}(r) - C_6/r^6 + \bar{V}_{\rm dd}(r)$. The first term is the centrifugal energy $\hbar^2\ell(\ell+1)/Mr^2$, the second one corresponds to the van der Waals interaction with $C_6 = 2003\ E_h a_0^6$ [38], with E_h being the Hartree energy, and the third term represents the leading effect of dipolar interaction at long distance. For the output channel, we use $\bar{V}_{\rm dd}(r) = -C_3/r^3$ with $C_3 = (6/7)\hbar^2 a_{\rm dd}/M$, which represents the angular average of $V_{\rm dd}(\boldsymbol{r})$ for the considered partial wave. For the input channel, this angular average vanishes. We therefore consider the next-order term, $\bar{V}_{\rm dd}(r) = -C_4/r^4$ with $C_4 = (147/160)\hbar^2 a_{\rm dd}^2/M$. This term results from second-order perturbation theory, considering the coupling between the input s-wave state and the d-wave states of the same spin multiplicity, with their splitting determined by the centrifugal energy [for details see [63] and references therein]. Note that the dipolar length $a_{\rm dd}$ is comparable to the length scale associated with the van der Waals interaction $R_6 = (MC_6/\hbar^2)^{1/4} = 156a_0$ [64]. Our perturbative treatment of $V_{\rm dd}$ holds for $r > a_{\rm dd} \approx R_6$. For smaller values of r, dipolar interactions should be handled in a nonperturbative manner, but they are small compared to van der Waals interactions and are expected to play a lesser role.

We numerically compute $\chi_{\rm i}$ and $\chi_{\rm f}$ by imposing a hard-core potential at short distances in the resolution of the Schrödinger equation, such that the total number of bound states equals the value 71 predicted in Ref. [65]. Quasi-identical results are obtained for $L_2^{\rm mix}$ with a Lennard-Jones potential with the same number of bound states, and also when the number of bound states is varied by $\pm 10\%$.

The evolution of $L_2^{\rm mix}$ with the magnetic field strongly depends on the interstate scattering length a_{78}. As shown in Fig. 2(b), we find good agreement with our experimental data for $a_{78} = 20$–$60a_0$. Furthermore, our results effectively exclude negative scattering length values or large positive values, $a_{78} \gtrsim 100a_0$, providing crucial information for determining the stability and miscibility regime of these samples. Note that our result does not verify $a_{78} = a_{88}$, as one would expect for pure contact interactions [66].

We apply the same method to the case of pure $|-7\rangle$ samples. In this case, we fit the atom number evolution by $N_0/(1 + L_2\bar{n}t)$, where $\bar{n}$ is the initial sample-averaged density and N_0 the initial atom number [see Fig. 2(c)]. As shown in Fig. 2(d), we also observe a nonmonotonic evolution of $L_2^{\rm pol}$ with B. In this case, there are two possible final channels, $|-7\rangle + |-8\rangle$ and $|-8\rangle + |-8\rangle$, each leading to a contribution analogous to Eq. (4). Therefore we do not expect that there exists a B field for which the total rate L_2 exactly cancels, which makes the determination of a_{77} by this method less accurate than for a_{78}. Using the same methodology, generalized to the case of losses resulting from the collision between two particles in state $|-7\rangle$ (see [55]), we extract the possible range for the scattering length $a_{77} = 40$–$120a_0$.

Interestingly, both loss rate minima are located at approximately the same magnetic field, $B = 2.5$ G, and equal to $L_{2,\rm min}^{\rm mix} = 0.26(25)\ \mu{\rm m}^3/{\rm s}$ and $L_{2,\rm min}^{\rm pol} = 0.9(2)\ \mu{\rm m}^3/{\rm s}$. These values correspond to an almost two-order of magnitude reduction compared to the Wigner law. Furthermore, the minimal value $L_{2,\rm min}^{\rm mix}$ is likely an overestimate, as it is derived from long probing times, during which one-body losses may contribute to the overall observed losses. At this magnetic field, we also measure the two-body relaxation rate for a pure BEC in $|-7\rangle$ and find $L_{2,\rm BEC} = 0.3(1)\ \mu{\rm m}^3/{\rm s}$, consistent with the expected twofold reduction due to the decreased two-body correlation function, at short range, for a BEC.

To confirm and improve on our determination of the scattering length a_{77}, we prepare a quasi-pure BEC in the internal state $|-7\rangle$ and analyze its expansion when it is released from the trap. The release occurs immediately after the transfer from $|-8\rangle$ to $|-7\rangle$ and we record the atomic

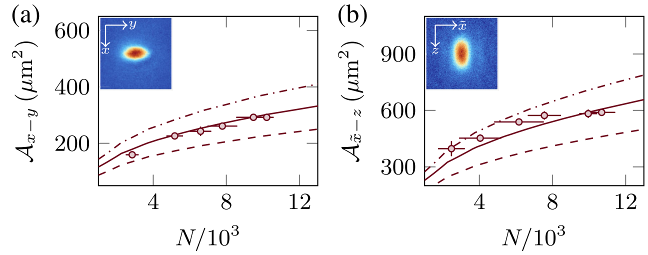

FIG. 3. Determination of the scattering length from time-of-flight expansion of a pure BEC in $|-7\rangle$ at a magnetic field $B = 1.43$ G. Area of the BEC, defined as the product of the Thomas-Fermi radii extracted from inverted parabola fits to absorption images, plotted as a function of atom number N in the (a) x–y and (b) $\tilde{x}$–z planes, with $\tilde{x}$ at a 70° angle from x and perpendicular to z. The lines correspond to numerical simulations for the BEC expansion, assuming scattering lengths of $a_{77} = 110a_0$ (solid line), $a_{77} = 98a_0$ (dashed line), and $a_{77} = 122a_0$ (dot-dash line). The trapping frequencies are $\{\omega_x, \omega_y, \omega_z\} = 2\pi \times \{100, 260, 200\}$ Hz.

density after a 13.1 ms TOF. Absorption imaging along two orthogonal axes allows us to observe the cloud expansion in all spatial directions. We show in Fig. 3 the variation of the cloud sizes after TOF as function of the atom number. The continuous lines show the prediction of a model based on the Castin-Dum scaling equations [67], here generalized to take into account dipolar interactions [68,69] (see also [55]). The comparison between numerical and experimental results gives $a_{77} = 110(10)a_0$, which is in agreement with the value inferred from the two-body loss rate (Fig. 2). As a sanity check, we repeated this experiment for a BEC prepared in $|-8\rangle$ and obtained $a_{88} = 136(8)a_0$, which agrees with published values [40,41]. Similarly we have measured the scattering length $a_{66} = 92(10)a_0$ (see [55]).

The determination of a_{77}, a_{88}, and a_{78} allows us to draw conclusions about the miscibility regime of this spin mixture. In the absence of dipolar interactions, the scattering length values would indicate that a mixture with equal populations in $|-8\rangle$ and $|-7\rangle$ is miscible, as it satisfies the inequality $a_{88}a_{77} \geq a_{78}^2$. However, the anisotropy of dipole-dipole interactions makes this conclusion more subtle. For a homogeneous 3D gas, we predict from the measured values of the three scattering lengths that the mixture is non miscible, because the head-to-tail arrangement of dipoles favors spatial separation of the two spin components [50]. In contrast, applying a strong confinement along the dipole orientation should lead to miscible mixtures [51]. Taking into account the reported scattering length values and our trap frequencies, it appears our system already lies in the miscible regime [70].

Alternatively, changing one of the aforementioned scattering lengths also gives access to different miscible regimes. To explore this aspect, we have identified spin-dependent Feshbach resonances near the dipolar relaxation minimum at $B \approx 2.5$ G. These resonances occur in a

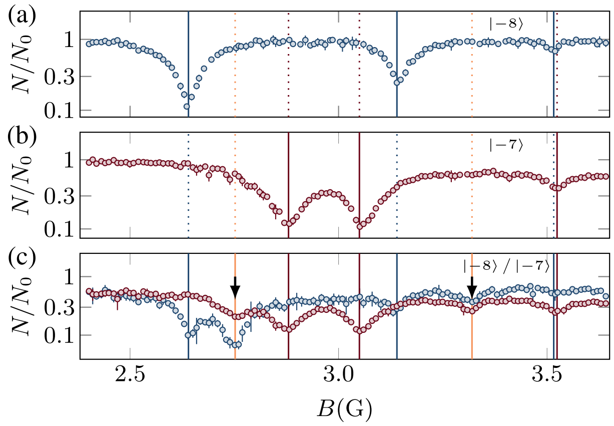

FIG. 4. Spin-dependent loss features following a 40 ms hold time at the target magnetic field. (a) Population variation with magnetic field for a pure BEC in $|-8\rangle$. (b) Population variation for a pure BEC in $|-7\rangle$. (c) Population variation for the case of a 50-50 spin mixture in $|-8\rangle$ (blue) and $|-7\rangle$ (red). The vertical lines represent the different spin-dependent Feshbach resonances. The vertical black arrows point to the interspecies loss features.

magnetic field region where dipolar relaxation processes are strongly suppressed (see [55]), ensuring the validity of our approach for exploring new phases of matter. We show in Fig. 4 the fraction of atoms remaining in the trap after a hold time of 40 ms, taking as initial state a pure BEC with adjustable fractions of $|-7\rangle$ and $|-8\rangle$. When all atoms are in $|-8\rangle$ [Fig. 4(a)], we recover the known three loss features described in Ref. [45] for this magnetic field range. When all atoms are in $|-7\rangle$ [Fig. 4(b)], we observe again three loss resonances, located at magnetic fields that differ from those for $|-8\rangle$.

The case of a 50%–50% spin-mixture case reveals extra features [Fig. 4(c)]. In addition to the resonances observed for pure $|-8\rangle$ and $|-7\rangle$ BECs, we observe two new features affecting both spin components. We interpret these losses as three-body recombination processes resulting from interspecies Feshbach resonances, involving two particles in a given spin state and another particle in a different spin state. We thus expect that the losses for the two states in an initial 50-50 mixture are at most in a ratio 2∶1, and reach equal values if the two processes $7+7+8$ and $7+8+8$ have equal probabilities. Here we find a ratio 1.5 and 0.8 between the losses for state $|-8\rangle$ and state $|-7\rangle$ for the two resonances of Fig. 4(c) at 2.75 and 3.3 G, respectively, which is compatible with the expected bound. Interestingly, these two resonances are located at magnetic fields equidistant from nearby intraspecies Feshbach resonances for $|-7\rangle$ and $|-8\rangle$.

In conclusion, our study represents a significant advancement in the preparation and stabilization of binary dipolar gases. We have identified a magnetic field region where two-body losses due to dipolar relaxation are reduced by nearly 2 orders of magnitude compared to the Wigner threshold law, making this system long-lived, similarly to its fermionic counterpart [28,35]. This result has allowed us to estimate both intra- and interspecies scattering lengths using a model based on single-channel scattering theory. A natural extension of our work is to develop a multichannel approach [36,71] to improve the accuracy of the determination of these scattering lengths from the measured relaxation rates. The exceptionally low two-body loss rate, observed near 2.5 G in a spin mixture of $|-7\rangle$ and $|-8\rangle$, combined with the identification of multiple inter- and intraspecies Feshbach resonances near this magnetic field, opens the possibility of studying various miscible regimes within this binary dipolar mixture. This development paves the way for exploring new quantum phases in dipolar gases.

Acknowledgments—We acknowledge fruitful discussions with the members of the Bose-Einstein condensate team at LKB, Bruno Laburthe-Tolra, and Luis Santos. We thank Sylvain Nascimbene for a careful reading of the manuscript. This research was funded, in part, by l'Agence Nationale de la Recherche (ANR), Projects No. ANR-20-CE30-0024 and No. ANR-24-CE30-7961. For the purpose of open access, the author has applied a CC-BY public copyright licence to any Author Accepted Manuscript (AAM) version arising from this submission. This work was also funded by Region Ile-de-France in the framework of DIM QuanTiP.

[1] M. A. Baranov, M. Dalmonte, G. Pupillo, and P. Zoller, Condensed matter theory of dipolar quantum gases, Chem. Rev. **112**, 5012 (2012).
[2] J. L. Bohn, A. M. Rey, and J. Ye, Cold molecules: Progress in quantum engineering of chemistry and quantum matter, Science **357**, 1002 (2017).
[3] A. Browaeys and T. Lahaye, Many-body physics with individually controlled Rydberg atoms, Nat. Phys. **16**, 132 (2020).
[4] L. Chomaz, I. Ferrier-Barbut, F. Ferlaino, B. Laburthe-Tolra, B. L. Lev, and T. Pfau, Dipolar physics: A review of experiments with magnetic quantum gases, Rep. Prog. Phys. **86**, 026401 (2022).
[5] N. Bigagli, W. Yuan, S. Zhang, B. Bulatovic, T. Karman, I. Stevenson, and S. Will, Observation of Bose-Einstein condensation of dipolar molecules, Nature (London) **631**, 289 (2024).
[6] L. Chomaz, R. M. van Bijnen, D. Petter, G. Faraoni, S. Baier, J. H. Becher, M. J. Mark, F. Waechtler, L. Santos, and F. Ferlaino, Observation of roton mode population in a dipolar quantum gas, Nat. Phys. **14**, 442 (2018).
[7] V. Makhalov, T. Satoor, A. Evrard, T. Chalopin, R. Lopes, and S. Nascimbene, Probing quantum criticality and symmetry breaking at the microscopic level, Phys. Rev. Lett. **123**, 120601 (2019).
[8] M. Guo, F. Böttcher, J. Hertkorn, J.-N. Schmidt, M. Wenzel, H. P. Büchler, T. Langen, and T. Pfau, The low-energy goldstone mode in a trapped dipolar supersolid, Nature (London) **574**, 386 (2019).

[9] L. Chomaz, D. Petter, P. Ilzhöfer, G. Natale, A. Trautmann, C. Politi, G. Durastante, R. M. W. van Bijnen, A. Patscheider, M. Sohmen, M. J. Mark, and F. Ferlaino, Long-lived and transient supersolid behaviors in dipolar quantum gases, Phys. Rev. X **9**, 021012 (2019).

[10] L. Tanzi, E. Lucioni, F. Famà, J. Catani, A. Fioretti, C. Gabbanini, R. N. Bisset, L. Santos, and G. Modugno, Observation of a dipolar quantum gas with metastable supersolid properties, Phys. Rev. Lett. **122**, 130405 (2019).

[11] F. Böttcher, J.-N. Schmidt, M. Wenzel, J. Hertkorn, M. Guo, T. Langen, and T. Pfau, Transient supersolid properties in an array of dipolar quantum droplets, Phys. Rev. X **9**, 011051 (2019).

[12] M. A. Norcia, C. Politi, L. Klaus, E. Poli, M. Sohmen, M. J. Mark, R. N. Bisset, L. Santos, and F. Ferlaino, Two-dimensional supersolidity in a dipolar quantum gas, Nature (London) **596**, 357 (2021).

[13] J.-N. Schmidt, J. Hertkorn, M. Guo, F. Böttcher, M. Schmidt, K. S. H. Ng, S. D. Graham, T. Langen, M. Zwierlein, and T. Pfau, Roton excitations in an oblate dipolar quantum gas, Phys. Rev. Lett. **126**, 193002 (2021).

[14] A. Recati and S. Stringari, Supersolidity in ultracold dipolar gases, Nat. Rev. Phys. **5**, 735 (2023).

[15] G. Biagioni, N. Antolini, B. Donelli, L. Pezzè, A. Smerzi, M. Fattori, A. Fioretti, C. Gabbanini, M. Inguscio, L. Tanzi, and G. Modugno, Measurement of the superfluid fraction of a supersolid by Josephson effect, Nature (London) **629**, 773 (2024).

[16] D. S. Petrov, Quantum mechanical stabilization of a collapsing Bose-Bose mixture, Phys. Rev. Lett. **115**, 155302 (2015).

[17] C. Cabrera, L. Tanzi, J. Sanz, B. Naylor, P. Thomas, P. Cheiney, and L. Tarruell, Quantum liquid droplets in a mixture of Bose-Einstein condensates, Science **359**, 301 (2018).

[18] K. Góral and L. Santos, Ground state and elementary excitations of single and binary Bose-Einstein condensates of trapped dipolar gases, Phys. Rev. A **66**, 023613 (2002).

[19] M. Arazo, A. Gallemí, M. Guilleumas, R. Mayol, and L. Santos, Self-bound crystals of antiparallel dipolar mixtures, Phys. Rev. Res. **5**, 043038 (2023).

[20] H. Saito, Y. Kawaguchi, and M. Ueda, Ferrofluidity in a two-component dipolar Bose-Einstein condensate, Phys. Rev. Lett. **102**, 230403 (2009).

[21] K.-T. Xi, T. Byrnes, and H. Saito, Fingering instabilities and pattern formation in a two-component dipolar Bose-Einstein condensate, Phys. Rev. A **97**, 023625 (2018).

[22] A.-C. Lee, D. Baillie, and P. B. Blakie, Excitations and phase ordering of the spin-stripe phase of a binary dipolar condensate, Phys. Rev. A **109**, 023323 (2024).

[23] S. Li, U. N. Le, and H. Saito, Long-lifetime supersolid in a two-component dipolar Bose-Einstein condensate, Phys. Rev. A **105**, L061302 (2022).

[24] T. Bland, E. Poli, C. Politi, L. Klaus, M. A. Norcia, F. Ferlaino, L. Santos, and R. N. Bisset, Two-dimensional supersolid formation in dipolar condensates, Phys. Rev. Lett. **128**, 195302 (2022).

[25] D. Scheiermann, L. P. Ardila, T. Bland, R. Bisset, and L. Santos, Catalyzation of supersolidity in binary dipolar condensates, Phys. Rev. A **107**, L021302 (2023).

[26] A. Trautmann, P. Ilzhöfer, G. Durastante, C. Politi, M. Sohmen, M. J. Mark, and F. Ferlaino, Dipolar quantum mixtures of erbium and dysprosium atoms, Phys. Rev. Lett. **121**, 213601 (2018).

[27] L. Santos and T. Pfau, Spin-3 chromium Bose-Einstein condensates, Phys. Rev. Lett. **96**, 190404 (2006).

[28] N. Q. Burdick, Y. Tang, and B. L. Lev, Long-lived spin-orbit-coupled degenerate dipolar Fermi gas, Phys. Rev. X **6**, 031022 (2016).

[29] S. Lepoutre, L. Gabardos, K. Kechadi, P. Pedri, O. Gorceix, E. Maréchal, L. Vernac, and B. Laburthe-Tolra, Collective spin modes of a trapped quantum ferrofluid, Phys. Rev. Lett. **121**, 013201 (2018).

[30] S. Baier, D. Petter, J. H. Becher, A. Patscheider, G. Natale, L. Chomaz, M. J. Mark, and F. Ferlaino, Realization of a strongly interacting Fermi gas of dipolar atoms, Phys. Rev. Lett. **121**, 093602 (2018).

[31] F. Claude, L. Lafforgue, J. J. A. Houwman, M. J. Mark, and F. Ferlaino, Optical manipulation of spin states in ultracold magnetic atoms via an inner-shell Hz transition, Phys. Rev. Res. **6**, L042016 (2024).

[32] C. Baroni, G. Lamporesi, and M. Zaccanti, Quantum mixtures of ultracold gases of neutral atoms, Nat. Rev. Phys. **6**, 736 (2024).

[33] S. Hensler, J. Werner, A. Griesmaier, P. Schmidt, A. Görlitz, T. Pfau, S. Giovanazzi, and K. Rzażewski, Dipolar relaxation in an ultra-cold gas of magnetically trapped chromium atoms, Appl. Phys. B **77**, 765 (2003).

[34] B. Pasquiou, G. Bismut, Q. Beaufils, A. Crubellier, E. Maréchal, P. Pedri, L. Vernac, O. Gorceix, and B. Laburthe-Tolra, Control of dipolar relaxation in external fields, Phys. Rev. A **81**, 042716 (2010).

[35] N. Q. Burdick, K. Baumann, Y. Tang, M. Lu, and B. L. Lev, Fermionic suppression of dipolar relaxation, Phys. Rev. Lett. **114**, 023201 (2015).

[36] S. Kotochigova, Controlling interactions between highly magnetic atoms with Feshbach resonances, Rep. Prog. Phys. **77**, 093901 (2014).

[37] A. Frisch, M. Mark, K. Aikawa, F. Ferlaino, J. L. Bohn, C. Makrides, A. Petrov, and S. Kotochigova, Quantum chaos in ultracold collisions of gas-phase erbium atoms, Nature (London) **507**, 475 (2014).

[38] T. Maier, H. Kadau, M. Schmitt, M. Wenzel, I. Ferrier-Barbut, T. Pfau, A. Frisch, S. Baier, K. Aikawa, L. Chomaz, M. J. Mark, F. Ferlaino, C. Makrides, E. Tiesinga, A. Petrov, and S. Kotochigova, Emergence of chaotic scattering in ultracold Er and Dy, Phys. Rev. X **5**, 041029 (2015).

[39] Y. Tang, A. Sykes, N. Q. Burdick, J. L. Bohn, and B. L. Lev, s-wave scattering lengths of the strongly dipolar bosons Dy^{162} and Dy^{164}, Phys. Rev. A **92**, 022703 (2015).

[40] Y. Tang, A. G. Sykes, N. Q. Burdick, J. M. DiSciacca, D. S. Petrov, and B. L. Lev, Anisotropic expansion of a thermal dipolar Bose gas, Phys. Rev. Lett. **117**, 155301 (2016).

[41] F. Böttcher, M. Wenzel, J.-N. Schmidt, M. Guo, T. Langen, I. Ferrier-Barbut, T. Pfau, R. Bombín, J. Sánchez-Baena, J. Boronat, and F. Mazzanti, Dilute dipolar quantum droplets

beyond the extended Gross-Pitaevskii equation, Phys. Rev. Res. **1**, 033088 (2019).

[42] V. A. Khlebnikov, D. A. Pershin, V. V. Tsyganok, E. T. Davletov, I. S. Cojocaru, E. S. Fedorova, A. A. Buchachenko, and A. V. Akimov, Random to chaotic statistic transformation in low-field Fano-Feshbach resonances of cold thulium atoms, Phys. Rev. Lett. **123**, 213402 (2019).

[43] A. Patscheider, L. Chomaz, G. Natale, D. Petter, M. J. Mark, S. Baier, B. Yang, R. R. W. Wang, J. L. Bohn, and F. Ferlaino, Determination of the scattering length of erbium atoms, Phys. Rev. A **105**, 063307 (2022).

[44] M. Krstajić, P. Juhász, J. Kučera, L. R. Hofer, G. Lamb, A. L. Marchant, and R. P. Smith, Characterization of three-body loss in Er 166 and optimized production of large Bose-Einstein condensates, Phys. Rev. A **108**, 063301 (2023).

[45] M. Lecomte, A. Journeaux, L. Renaud, J. Dalibard, and R. Lopes, Loss features in ultracold ^{162}Dy gases: Two- versus three-body processes, Phys. Rev. A **109**, 023319 (2024).

[46] S. Lepoutre, J. Schachenmayer, L. Gabardos, B. Zhu, B. Naylor, E. Maréchal, O. Gorceix, A. M. Rey, L. Vernac, and B. Laburthe-Tolra, Out-of-equilibrium quantum magnetism and thermalization in a spin-3 many-body dipolar lattice system, Nat. Commun. **10**, 1714 (2019).

[47] P. Barral, M. Cantara, L. Du, W. Lunden, J. de Hond, A. O. Jamison, and W. Ketterle, Suppressing dipolar relaxation in thin layers of dysprosium atoms, Nat. Commun. **15**, 3566 (2024).

[48] J. Weiner, V. S. Bagnato, S. Zilio, and P. S. Julienne, Experiments and theory in cold and ultracold collisions, Rev. Mod. Phys. **71**, 1 (1999).

[49] C. Chin, R. Grimm, P. S. Julienne, and E. Tiesinga, Feshbach resonances in ultracold gases, Rev. Mod. Phys. **82**, 1225 (2010).

[50] R. M. Wilson, C. Ticknor, J. L. Bohn, and E. Timmermans, Roton immiscibility in a two-component dipolar Bose gas, Phys. Rev. A **86**, 033606 (2012).

[51] R. K. Kumar, L. Tomio, B. A. Malomed, and A. Gammal, Vortex lattices in binary Bose-Einstein condensates with dipole-dipole interactions, Phys. Rev. A **96**, 063624 (2017).

[52] S. Halder, S. Das, and S. Majumder, Two-dimensional miscible-immiscible supersolid and droplet crystal state in a homonuclear dipolar bosonic mixture, Phys. Rev. A **107**, 063303 (2023).

[53] M. Wickliffe, J. E. Lawler, and G. Nave, Atomic transition probabilities for Dy I and Dy II, J. Quant. Spectrosc. Radiat. Transfer **66**, 363 (2000).

[54] H. Li, J.-F. Wyart, O. Dulieu, S. Nascimbene, and M. Lepers, Optical trapping of ultracold dysprosium atoms: Transition probabilities, dynamic dipole polarizabilities and van der Waals C_6 coefficients, J. Phys. B **50**, 014005 (2017).

[55] See Supplemental Material at http://link.aps.org/supplemental/10.1103/PhysRevLett.134.013402 for discussing the characterization of the optical transition at 530.3 nm, preparation of the Raman transitions, theoretical description of two-body loss rate due to the dipolar relaxation, determination of the background scattering length from the expansion of a dipolar BEC, identification of loss features for the two lowest energy Zeeman sublevels, dependence of the two-body loss rate on the scattering length, and determination of L_2 from experimental data.

[56] C. Ravensbergen, V. Corre, E. Soave, M. Kreyer, S. Tzanova, E. Kirilov, and R. Grimm, Accurate determination of the dynamical polarizability of dysprosium, Phys. Rev. Lett. **120**, 223001 (2018).

[57] T. Chalopin, V. Makhalov, C. Bouazza, A. Evrard, A. Barker, M. Lepers, J.-F. Wyart, O. Dulieu, J. Dalibard, R. Lopes, and S. Nascimbene, Anisotropic light shift and magic polarization of the intercombination line of dysprosium atoms in a far-detuned dipole trap, Phys. Rev. A **98**, 040502(R) (2018).

[58] C. Cohen-Tannoudji, B. Diu, and F. Laloe, *Quantum Mechanics* (Wiley-VCH, Weinheim, 1986), Vol. 2.

[59] A. R. Edmonds, *Angular Momentum in Quantum Mechanics* (Princeton University Press, Princeton, NJ, 1996), Vol. 4.

[60] A. Moerdijk and B. Verhaar, Collisional two-and three-body decay rates of dilute quantum gases at ultralow temperatures, Phys. Rev. A **53**, R19(R) (1996).

[61] S. Yi and L. You, Trapped condensates of atoms with dipole interactions, Phys. Rev. A **63**, 053607 (2001).

[62] J. Bohn, M. Cavagnero, and C. Ticknor, Quasi-universal dipolar scattering in cold and ultracold gases, New J. Phys. **11**, 055039 (2009).

[63] T. Maier, I. Ferrier-Barbut, H. Kadau, M. Schmitt, M. Wenzel, C. Wink, T. Pfau, K. Jachymski, and P. S. Julienne, Broad universal Feshbach resonances in the chaotic spectrum of dysprosium atoms, Phys. Rev. A **92**, 060702(R) (2015).

[64] B. Gao, General form of the quantum-defect theory for $-1/r^{\alpha}$ type of potentials with $\alpha > 2$, Phys. Rev. A **78**, 012702 (2008).

[65] A. Petrov, E. Tiesinga, and S. Kotochigova, Anisotropy-induced Feshbach resonances in a quantum dipolar gas of highly magnetic atoms, Phys. Rev. Lett. **109**, 103002 (2012).

[66] Y. Kawaguchi and M. Ueda, Spinor Bose–Einstein condensates, Phys. Rep. **520**, 253 (2012).

[67] Y. Castin and R. Dum, Bose-Einstein condensates in time dependent traps, Phys. Rev. Lett. **77**, 5315 (1996).

[68] D. H. J. O'Dell, S. Giovanazzi, and C. Eberlein, Exact hydrodynamics of a trapped dipolar Bose-Einstein condensate, Phys. Rev. Lett. **92**, 250401 (2004).

[69] C. Eberlein, S. Giovanazzi, and D. H. J. O'Dell, Exact solution of the Thomas-Fermi equation for a trapped Bose-Einstein condensate with dipole-dipole interactions, Phys. Rev. A **71**, 033618 (2005).

[70] D. Scheiermann, A. Gallemí, and L. Santos, Excitation spectrum of a double supersolid in a trapped dipolar Bose mixture, arXiv:2412.05215 (2024).

[71] T. Secker, J.-L. Li, P. M. A. Mestrom, and S. J. J. M. F. Kokkelmans, Multichannel nature of three-body recombination for ultracold K 39, Phys. Rev. A **103**, 022825 (2021).